Integral Equation Methods for Vortex Dominated Flows, a High-order Conservative Eulerian Approach

J. Bevan, UIUC

ICERM/HKUST Fast Integral Equation Methods
January 5, 2016

Vorticity and Circulation

$$\omega = \nabla \times \mathbf{u} \tag{1}$$

$$\Gamma = \oint_{\partial S} \mathbf{u} \cdot d\mathbf{l} = \iint_S \omega \cdot d\mathbf{S} \tag{2}$$

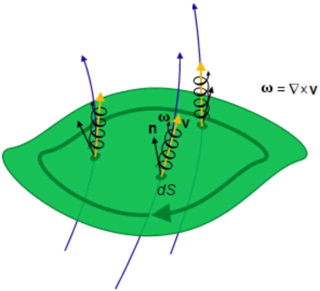

[0] https://commons.wikimedia.org/wiki/File:Generalcirculation-vorticitydiagram.svg

Physical Examples and Motivating Problems

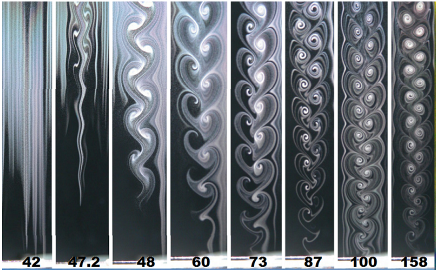

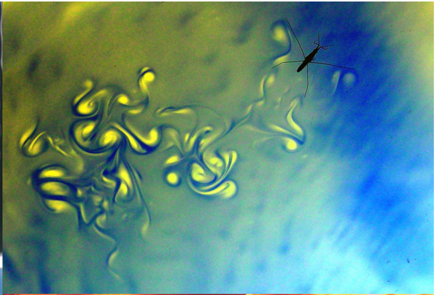

Motivation

- Direct solution of Navier-Stokes impractical for many fluid problems
- Vorticity-velocity formulation well-suited for inviscid, incompressible, vortex dominated flows
- Lagrangian vortex methods are common approach[1,2], but face several challenges[3]
- Initial vortex points become disorganized, re-meshing etc. required
- Eulerian approach avoids disorganization, extendable to high order
- Brown et al. successful with Eulerian approach for low order FVM[4] suggests high-order extension possible

[1] J. Strain. Fast adaptive 2D vortex methods. Journal of computational physics 132.1 (1997): 108-122.

[2] Moussa, C., Carley, M. J. (2008). A Lagrangian vortex method for unbounded flows. International journal for numerical methods in fluids, 58(2), 161-181.

[3] J. Strain. 2D vortex methods and singular quadrature rules. Journal of Computational Physics 124.1 (1996): 131-145.

[4] R.E. Brown. Rotor Wake Modeling for Flight Dynamic Simulation of Helicopters. AIAA Journal, 2000. Vol. 38(No. 1): p. 57-63.

Goals of Technique

Goals:

- Development of a high-order solver for inviscid incompressible vorticity-dominated flows in 2D
  - High-order advective solver capable of mixed order flux handling
  - High-order Biot-Savart evaluation routine

Contributions:

- Complete high-order method for velocity-vorticity inviscid flow
- Validation of solver and underlying Eulerian vortex approach
- Evaluation of convergence, error, and performance of method and solver

Proposed Method

- Eulerian representation of velocity and vorticity
- Solution of inviscid velocity-vorticity PDE
- Velocity evaluation via eval of integral equation (v.s. sol'n of PDE)[5]
- Vorticity advection via a line-DG[6] approach
- Method of lines, explicit time-stepping with Runge-Kutta[7]

[5] Winckelmans, G. S., and A. Leonard. Contributions to vortex particle methods for the computation of three-dimensional incompressible unsteady flows. Journal of Computational Physics 109.2 (1993): 247-273.

[6] P.O. Persson. A Sparse and High-Order Accurate Line-Based Discontinuous Galerkin Method for Unstructured Meshes. J. Comp. Phys., Vol. 233, pp. 414-429, Jan 2013.

[7] Niegemann, Jens, Richard Diehl, and Kurt Busch. Efficient low-storage Runge–Kutta schemes with optimized stability regions. Journal of Computational Physics 231.2 (2012): 364-372.

Theory: Navier-Stokes: Velocity-vorticity form

Navier-Stokes momentum equation

$$\rho\left(\frac{\partial \mathbf{u}}{\partial t} + \mathbf{u}\cdot\nabla\mathbf{u}\right) = -\nabla p + \mu\nabla^2\mathbf{u} + \tfrac{1}{3}\,\mu\nabla(\nabla\cdot\mathbf{u}) \qquad (3)$$

where u is the velocity field, p is the pressure field, and ρ is the density. Define *vorticity* as

$$\omega = \nabla\times\mathbf{u} \qquad (4)$$

Navier-Stokes can be recast as

$$\frac{\partial \omega}{\partial t} + \mathbf{u}\cdot\nabla\omega - \omega\cdot\nabla\mathbf{u} = S(x,t) \qquad (5)$$

viscous generation of vorticity, S

Velocity-vorticity form

Advantages:

- Explicit conservation of vorticity.
- Frequently distribution of the vorticity is sparse.
- No pressure term.

Simplified in 2D, vortex stretching zero. Express in terms of vortex flux $f_i(\omega) = u_i\,\omega$

$$\frac{\partial \omega}{\partial t} + \frac{\partial f}{\partial x_i} = S(x,t) \tag{6}$$

Velocity Evaluation

For incompressible flows velocity related to vorticity by

$$\nabla^2 u = -\nabla \times \omega \tag{7}$$

Invert to obtain Biot-Savart integral

$$u(x^*) = \int_\Omega K(x^*, x) \times \omega(x) dx \tag{8}$$

x^* is velocity eval point, x is non-zero vorticity domain, $K(x^*, x)$ singular Biot-Savart kernel[8]

$$K(x^*, x) = \frac{-1}{2\pi} \frac{x^* - x}{|x^* - x|^2} \tag{9}$$

---

[8] Beale, J. Thomas, and Andrew Majda. High order accurate vortex methods with explicit velocity kernels. Journal of Computational Physics 58.2 (1985): 188-208.

Kernel De-singularization: Two Viewpoints

- Lagrangian: Singularity in Biot-Savart kernel generates non-physical velocities near vortex points, de-singularize by approximation of Dirac delta function using finite cutoff radius δ.
- Lagrangian: Heuristically, one deals with vortex “blobs”.
- Eulerian: Vorticity is not confined to points, but spatially varying; what purpose does de-singularization serve? Strictly practical.
- Eulerian: While Biot-Savart kernel converges analytically, no guarantees numerically. Quadrature assumes polynomial basis appropriate approximation.
- Eulerian: De-singularization means to an end, improve quadrature convergence qualities.

Convergence of Biot-Savart Integral

- Nearly singular nature of Biot-Savart kernel difficult to integrate numerically
- Smaller the cutoff radius, larger quadrature errors
- Larger cutoff radius, larger velocity approximation errors
- Cutoff radius should be selected to balance both

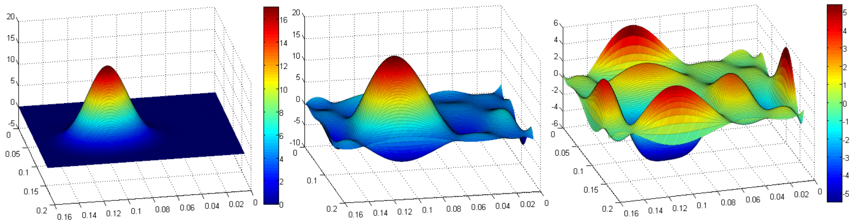

Discontinuous Galerkin (DG)

- Why DG vs others?

We seek to solve the PDE Eqn. (6). An approximate solution $\widetilde{\omega}$ has residual

$$\frac{\partial \widetilde{\omega}}{\partial t} + \frac{\partial f}{\partial x_i} = R(x) \tag{10}$$

1-D case, vorticity sources omitted for simplicity.

DG approach[9]: minimize the L^2 norm by orthogonal projection of residual onto approximating space. Complete basis made from test functions ϕ_j, so:

$$\int_\Omega R(x)\phi_j \, dx = 0 \quad \text{for all } j \tag{11}$$

Substituting residual with conservation PDE yields:

$$\int_\Omega \frac{\partial \widetilde{\omega}}{\partial t} \phi_j \, dx + \int_\Omega \frac{\partial f(\widetilde{\omega})}{\partial x} \phi_j \, dx = 0 \quad \text{for all } j \tag{12}$$

[9] W.H Reed and T.R. Hill. Triangular mesh methods for the neutron transport equation. 1973.

Discontinuous Galerkin (DG)(cont.)

Use same space for both test functions and and approximation, so Mth order vorticity approximation is

$$\omega(x,t) \approx \widetilde{\omega}(x,t) = \sum_{i=0}^{M} a_i(t)\psi_i(x) \tag{13}$$

Substitute into Eqn. (12) and integrate by parts second term:

$$\sum_{i=0}^{M} \left[\frac{da_i(t)}{dt} \int_{x_L}^{x_R} \psi_i(x)\, \phi_j(x)\; dx \right] + f\phi_j(x)\Big|_{x_L}^{x_R} - \int_{x_L}^{x_R} f(\widetilde{\omega})\, \frac{d\phi_j(x)}{dx}\; dx = 0 \tag{14}$$

Note: Local solution to PDE on an element.

Discontinuous Galerkin (DG)(cont.)

All local solutions decoupled, also vorticity multiply defined at overlapping element boundaries. Recover global solution and treat element boundaries via an upwind flux function[10](similar to finite volume method)

$$\hat{f}_{upwind}(x^+, x^-) = u\{\{\widetilde{\omega}\}\} + \frac{|u|}{2}[[\widetilde{\omega}]] \tag{15}$$

where $\{\{\omega^+\}\} = \frac{\omega^+ + \omega^-}{2}$ and $[[\omega]] = \omega^+ - \omega^-$

Applying change of variables to map to arbitrary computational element $X \in [-1, 1]$ results in:

$$\frac{\Delta x}{2} \sum_{i=0}^{M} \left[\frac{da_i}{dt} \int_{-1}^{1} \psi_i \, \phi_j \; dX \right] + \hat{f} \phi_j \Big|_{x_L}^{x_R} - \int_{-1}^{1} f(\widetilde{\omega}) \, \frac{d\phi_j}{dX} \; dX = 0 \tag{16}$$

[10] Hesthaven, Jan S., and Tim Warburton. Nodal discontinuous Galerkin methods: algorithms, analysis, and applications. Vol. 54. Springer Science & Business Media, 2007.

Solver Overview

```
Define problem parameters
Define solver parameters
Calculate derived solver parameters
Setup intitial conditions
Initialize solver
%Time stepping
for t=0 to end
   if datalog?=yes
      save system state to file and plot
   end
   %Loop through RK stages
   for s=1 to last_stage
      %For elements above threshold
      for each vorticity source
         calculate velocity contributions
      end
      %Calculate semi-discrete system terms
      interpolate boundary_vorticity
      calculate numerical_fluxes
      calculate total_surface_flux
      calculate internal_stiffness_flux

      vorticity_rate_of_change=...
         internal_stiffness_flux - total_surface_flux

      RK_stage= (RK_coeff_a*RK_stage) +...
         (time_step * vorticity_rate_of_change)
      vorticity= vorticity + RK_coeff_b * RK_stage
   end
end
```

Methodology: Method Specific Choices

- Choose basis functions to be the interpolating Lagrange polynomials

$$\psi_i(x) = \ell_i(x) = \prod_{\substack{p=0 \\ p\neq i}}^{M} \frac{x - x_p}{x_i - x_p} \tag{17}$$

- Choose vorticity interpolation nodes to be the Gauss-Legendre points, collocate with quadrature points, results in simplification of mass matrix

$$\int \ell_i(x)\ell_j(x)dx = \delta_{ij} w_j \tag{18}$$

- Take line-DG[6] approach, form 2D basis as tensor product of 1D bases

$$f(x,y) \approx \left[\sum_{j=0}^{L} z_j \ell_j(y)\right] \times \left[\sum_{i=0}^{M} z_i \ell_i(x)\right] = \sum_{j=0}^{M}\sum_{i=0}^{M} z_{ij}\ell_j\ell_i = \sum_{j=0}^{M} z_{ij}\ell_j \sum_{i=0}^{M} \ell_i \tag{19}$$

Method Specific Choices(cont.)

- The PDE is now solved along each tensor direction

$$\frac{\Delta x}{2}\sum_{i=0}^{M}\left[\frac{dz_{ij}}{dt}\int_{-1}^{1}\ell_i\,\ell_j\;dX\right]+\hat{f}\ell_j\Big|_{x_L}^{x_R}-\int_{-1}^{1}f(\widetilde{\omega})\,\ell_j'\;dX=0 \tag{20}$$

- The rate of change at each node is the sum of the contribution along each tensor direction

$$\frac{\partial\omega_{ij}}{\partial t}=(\frac{\partial\omega_{ij}}{\partial t})_{x-line}+(\frac{\partial\omega_{ij}}{\partial t})_{y-line} \tag{21}$$

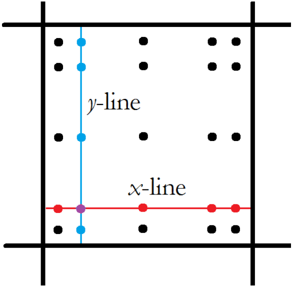

Velocity Evaluation

- Calculate velocity at all velocity nodes by summation of contribution from all vorticity using de-singularized kernel and Gauss-Legendre quadrature

$$u(x^*) = \sum_{E=1}^{N_{mask}} [\omega_{pre}]^T K_\delta(x^* - [x_E]) \tag{22}$$

$$\omega_{pre} = [\omega(x_E)].*[w_i \otimes w_j] \tag{23}$$

- Pre-multiplication of particular elemental vorticity source by outer product of Gauss-Legendre quadrature weights and computing as vector-vector product saves great deal of computational effort.
- Kernel values pre-calculated for "generalized" reference frame

Explicit Time-Stepping

- Method of lines approach to semi-discrete system
- Low-storage explicit Runge-Kutta method used
- 14 stage-4th order "NRK14C" used to maximize stable time-step[7]
- Stability region almost 1.9 times larger per stage along negative real axis, chief consideration for dissipative upwind DG schemes

Results: Validating Test Cases

- Perlman: Stationary vortex[11]

$$\omega(z) = (1-|z|^2)^7,\ |z| \le 1 \quad \omega(z) = 0,\ |z| > 1 \quad z^2 = x^2 + y^2 \tag{24}$$

- Has analytical solution to vorticity and velocity fields

$$u(z,t) = f(|z|)\begin{pmatrix} y \\ -x \end{pmatrix} \tag{25}$$

where

$$f(|z|) = \begin{cases} -\frac{1}{16|z|^2}(1-(1-|z|^2)^8) & |z| \le 1 \\ -\frac{1}{16|z|^2} & |z| > 1 \end{cases}$$

[11] M. Perlman. On the accuracy of vortex methods, J. Comput. Phys. 59 (1985) 200–223.

Comparison of Cutoff Radius Effects(P)

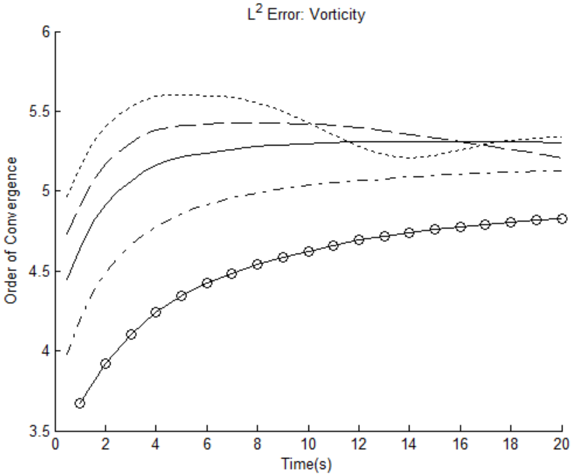

Figure: Comparison of convergence effects on vorticity by cutoff radius for $\delta/\Delta x$=0.1(..), 0.2(- -), 0.3(-), 0.5(-.), 0.9(-o).

Comparison of Cutoff Radius Effects(P)(cont.)

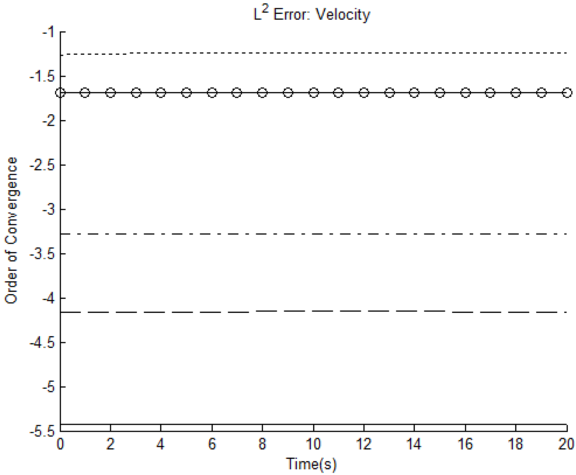

Figure: Comparison of convergence effects on velocity by cutoff radius for $\delta/\Delta x$=0.1(..), 0.2(- -), 0.3(-), 0.5(-.), 0.9(-o).

Observed Convergence Rate of Various Orders(P)

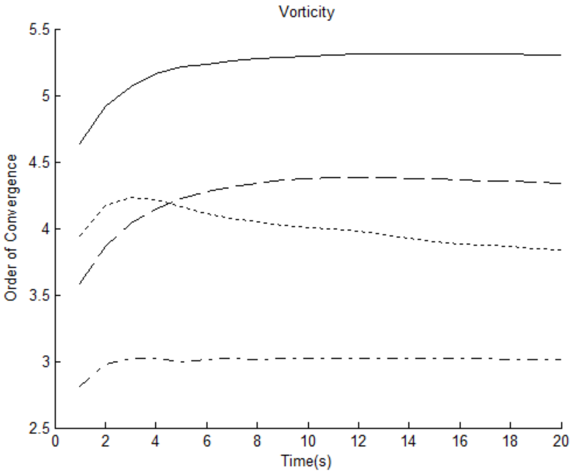

Figure: Comparison of convergence rate for various order methods: 3rd(-.), 4th(..), 5th(- -), and 6th(-).

Validating Test Cases

- Strain: Interacting vortex patches[12]

$$\omega(x,y,0) = \sum_{j=1}^{m} \Omega_j exp(-((x-x_j)^2 + (y-y_j)^2)/\rho_j^2) \quad (26)$$

Table: Interacting Vortex Patch Parameters

j	x_j	y_j	ρ_j	Ω_j
1	-0.6988	-1.7756	0.6768	-0.4515
2	1.4363	-1.4566	0.3294	0.4968
3	-0.1722	0.4175	0.5807	-0.9643
4	-1.5009	-0.0937	0.2504	0.3418

[12] J. Strain. 2D vortex methods and singular quadrature rules. Journal of Computational Physics 124.1 (1996): 131-145.

Strain Test Case, t=0

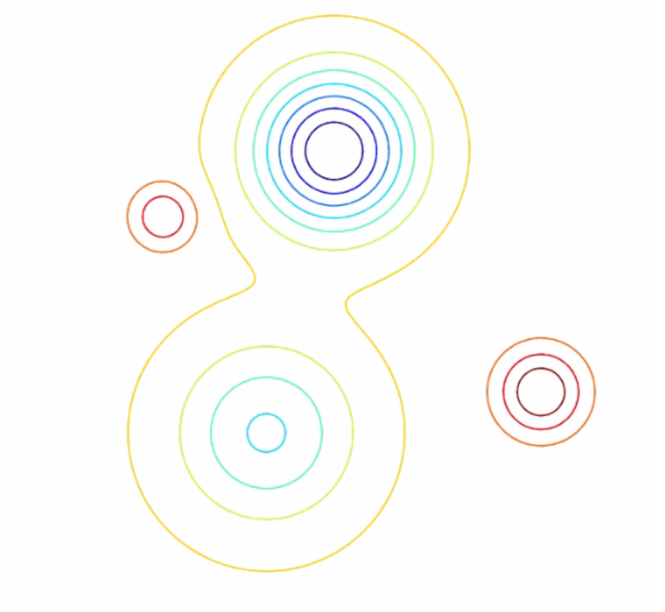

Approximated Convergence Rate(S)

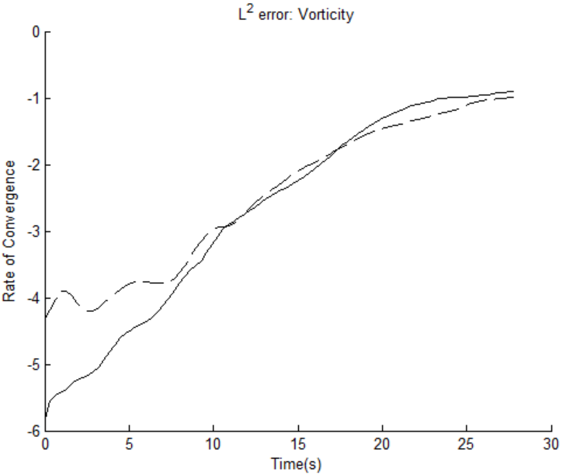

Figure: Dependency of rate of convergence on order of method, for a 4th order(- -) and 6th order(-) method.

Approximated Convergence Rate(S)(cont.)

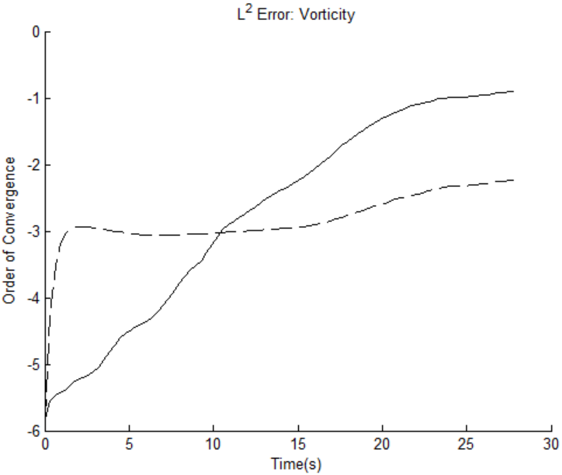

Figure: Dependency of rate of convergence on cutoff radius in sixth order method, for a $\delta/\Delta x=$ 0.5(- -) and 0.25(-).

Qualitative Comparison w/ Previous Work[12]

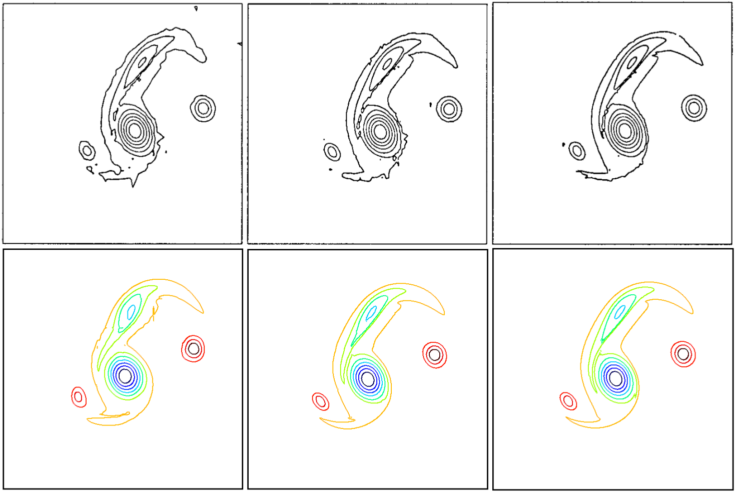

Figure: Comparison of Strain's results with present method t=28. Left to right, top to bottom, DOF= 6400, 12800, 25600; 3136, 7056, 63504. Reprinted with permission from Elsevier.

Validating Test Cases

- Koumoutsakos: Elliptical vortex[13]

$$\omega^{II}(x,y,0)_{mod} = 20(1-((x/a)^2+(y/b)^2)^2/0.8^4) \quad a=1,\ b=2 \tag{27}$$

[13] P. Koumoutsakos. Inviscid axisymmetrization of an elliptical vortex, J. Comput. Phys. 138 (1997) 821–857.

Qualitative Comparison of Vorticity(K)

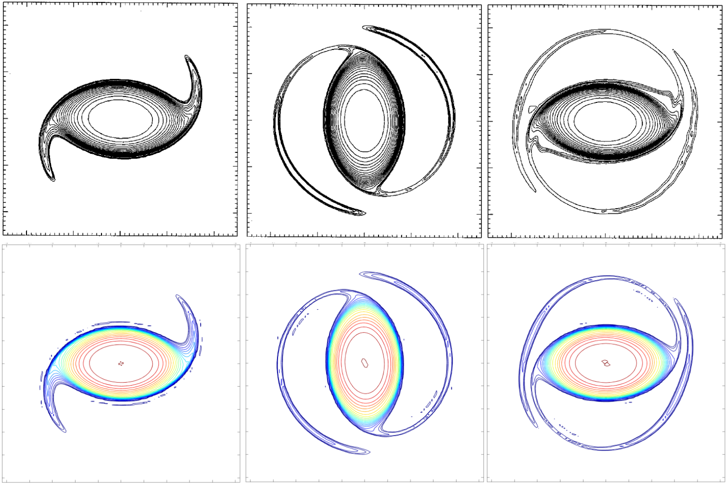

Figure: Comparison of vorticity, Koumoutsakos (top) and present method (bottom). From left to right, top to bottom t=1, 2, 4; 0.80, 1.93, 2.32. Reprinted with permission from Elsevier.

Qualitative Comparison of Vorticity(K)(cont.)

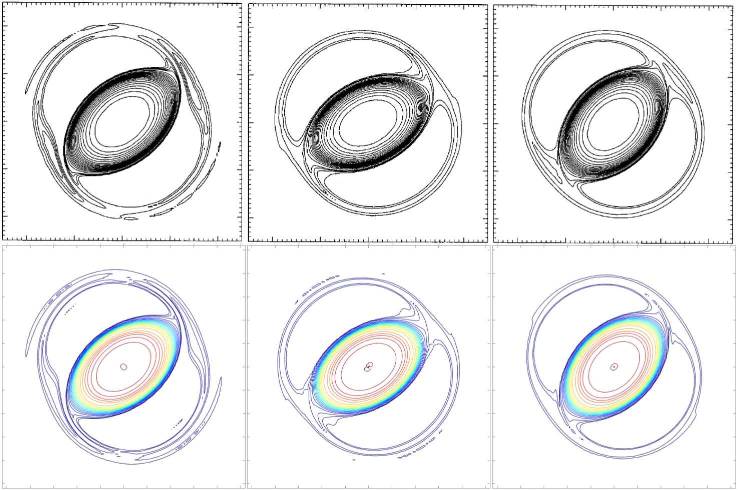

Figure: Comparison of vorticity, Koumoutsakos (top) and present method (bottom). From left to right top to bottom,: t=6, 12, 18; 5.94, 11.99, 17.94. Reprinted with permission from Elsevier.

Qualitative Comparison of Vorticity(K)(cont.)

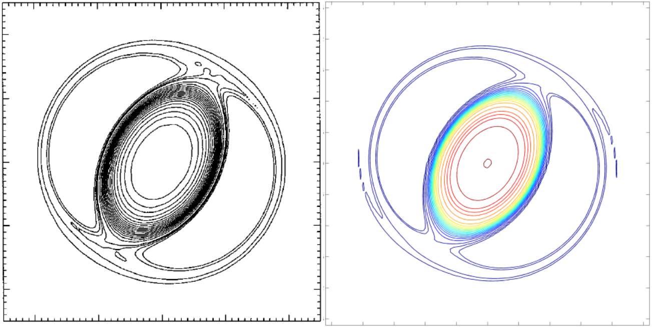

Figure: Comparison of vorticity, Koumoutsakos (left) and present method (right). From left to right: t=24; 23.98. Reprinted with permission from Elsevier.

Comparison of Aspect Ratio(K)

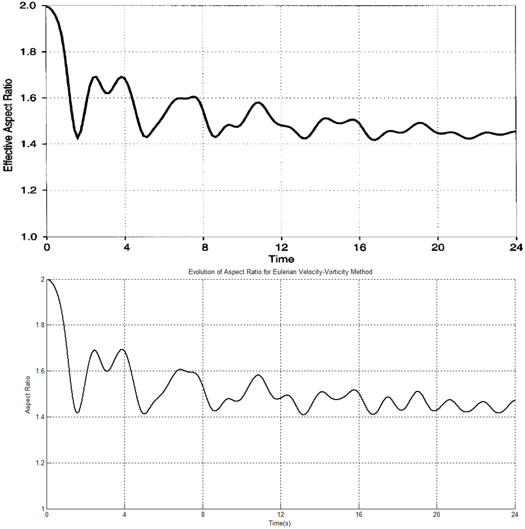

Figure: Comparison of effective aspect ratio, Koumoutsakos (top) and present method (bottom). Reprinted with permission from Elsevier.

Discussion: Validation

- Analytical: With proper choice of kernel, cutoff radius, stage-wise velocity evaluation, and matching velocity order method able to obtain solution within discretization error of exact solution for velocity and vorticity.
- Qualitative: Excellent agreement in Strain test case even for test with far fewer DOFs
- Good agreement in Koumoutsakos test case, with some minor deviation towards end of period studied and minor artifacting at vortex body boundaries.
- DOFs required about equal to Koumoutsakos's results, despite being higher-order method.
- Arm filaments and vortex body boundary challenging for polynomial basis functions, discontinuous derivatives affect bound on interpolation error.

Convergence Rate

- In Perlman test case, capable of near optimal convergence rates for stationary vortex test case.
- Half-order less convergence rate for higher order methods due to lack of as many vorticity derivatives.
- Non-optimal approximated convergence observed in Strain test case.
- Choice of two options, cutoff radius too small and gradual decay of convergence to first order from optimal. Cutoff radius too large, constant but non-optimal order of convergence.
- Tempting to blame smallest feature size or challenging evolution evolution for convergence, but testing with pairs of Perlman vortices shows same issues.

Exact Biot-Savart Integration

- Ideally: More accurately integrate B-S kernel, w/o extra error from de-singularization approximation.
- Example: Calculate velocity component at particular point:

$$u_y(T_x) = \int\int \frac{\mathbf{x} - T_x}{2\pi r^2} \omega(\mathbf{x}) d\mathbf{x} \tag{28}$$

- ω is actually Lagrange interpolation of vorticity (with interp. values z_{ij}), so substitute:

$$u_y(T_x) = \frac{1}{2\pi} \sum_i \sum_j z_{ij} \int\int \frac{x - T_x}{r^2}\, \ell_i(x)\ell_j(y)\; dx\; dy \tag{29}$$

- Note: Variable part of interp. occurs outside integral. We can pre-calculate integrals for all combinations and store.
- Yields modified quadrature:

$$u(T_-) = \frac{1}{2\pi} \sum_i \sum_j z_{ij} W_{(-,T_x,T_y,i,j)} \tag{30}$$

Exact B-S Integr.: Modified Kernel Values

- How do these weights vary spatially wrt target point? Divide special weights by tensor product of standard Gauss-Legendre:

$$u_x = \frac{1}{2\pi} \sum_i \sum_j z_{ij} \frac{W_{(i,j)}}{W_{GL}} W_{GL} \tag{31}$$

- Note: Can break into two parts; ω interpolation (z_{ij}) and B-S kernel values. Heuristically:

$$u_x = \frac{1}{2\pi} \sum_i \sum_j z_{ij} \widetilde{k}_{ij} W_{GL} \tag{32}$$

- We have recovered something that looks like "modified" kernel values. How do they vary spatially?

Exact B-S Integr.: Modified Kernel Values(cont.)

- Modifications to standard kernel values are local; neighboring/adjacent elements. Promising for FMM acceleration.

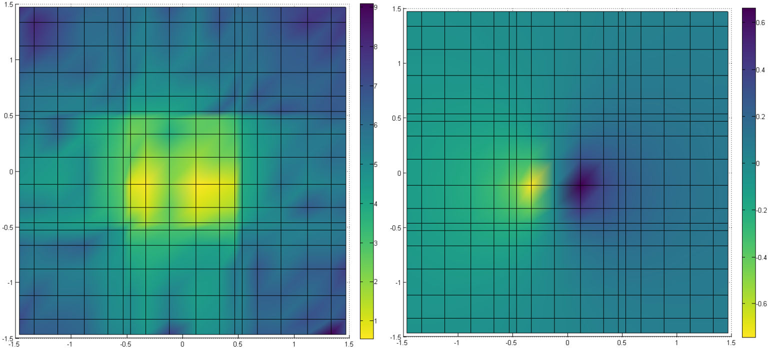

Figure: Number of digits in common between modified and original kernel(left), original kernel values(right); 5th order nodal set.

Exact B-S Integr.: Modified Kernel Values(cont.)

- Apply modified scheme to same Strain test case previously studied, but now with exact kernel integration.

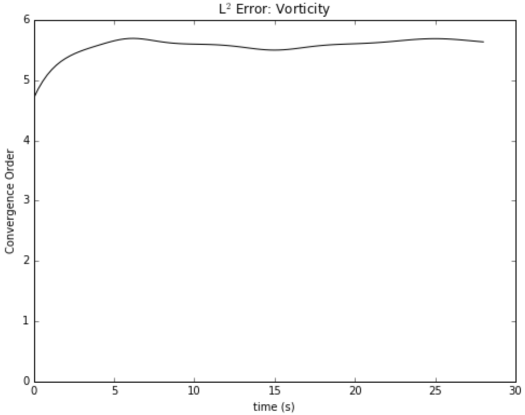

Figure: Dramatically improved convergence order with exact kernel integration scheme, same parameters as previous Stain test case plots.

Modified Kernel Scheme Drawbacks, and Future Directions

- Drawback: Calculation/storage of modified kernel values for unstructured meshes non-trivial
- Drawback: Curse of dimensionality causes explosion of number of modified kernel values necessary for even moderate orders for 3-D problems.
- Alternate approach: Use QBX for evaluation of singular Biot-Savart integral.
- Requires: Volume QBX evaluation. What is the proper choice of kernel where expansion "center" can be both "close" to the target point, but sufficiently smoother to achieve high-order scheme.
- Requires: Fast algorithm version for unstructured meshes needs FMM capable of dealing with interplay between mesh elements (and associated discretizations) and the (potentially adaptive) FMM tree.